The Far Wings of the GHRS PSF

A.B. Schultz, S. Hulbert, L. Sherbert, and D. Soderblom
September 21, 1997

ABSTRACT

The GHRS Point Spread Function (PSF) was measured directly by stepping (dwell scan) the Small Science Aperture across the star HD106343 (program ID: 6210) using the G160M and G270M gratings. Two scan directions were sampled, along the instrument –x-axis at wavelengths 1400 Å and 2700 Å, and along the +y-axis at 2700 Å. The scan steps were spaced 0.4 arcsecond apart and went out to a radius of 3.0 arcsec from the star. RAPID mode (sample time of 1 second) was used to measure the counts at each dwell position. Nine points (9) were extracted from the data to define the PSF envelope. The PSF exhibits a low intensity side lobe peaking at a radial distance of ~2.0 arcsecond.

1. The Post-COSTAR Point Spread Function

The GHRS Point Spread Function (PSF) was measured after deployment of COSTAR in December 1993. The post-COSTAR PSF has a sharp core and weak wings. Observations through the Small Science Aperture (SSA) show a Gaussian core with a FWHM of 0.975 diodes and wings that fall off (in intensity) as r^{-3} at radii larger than 1 arcsec. When this measured profile was deconvolved from the square SSA aperture, a sharp core was found with a FWHM of ~0.375 diodes, corresponding to about 0.08 arcsec. In the far wings of the PSF (beyond 0.5 arcsec), the intensity appears to fall off as a power law, with a slope of –3.15. The PSF was found to have significant asymmetries. See Robinson, R., *"Investigating the Post-COSTAR Point Spread Function for the GHRS"* in Calibrating Hubble Space Telescope: Post Servicing Mission, 1995 for a detailed description of the analysis of the PSF.

During preflight testing of COSTAR, the GHRS mirrors were contaminated by fine dust particles. Light scattering was expected to be a problem at the radial distance of 2 to 3 arcsec. The first Servicing Mission Orbital Verification (SMOV) observations agreed moderately with the light scattering theoretical expectations.

SMOV calibration program 5745 concentrated on the central region of the PSF, while program 4781 sampled the PSF out to a radial distance of 3.2 arcsec. Program 4781 data

were obtained at 1450 Å. The goal of Cycle 5 calibration program 6210 was to measure the far wings of the PSF at large radial distances, and to overlap with the observations of program 4781. Two central wavelengths were chosen, 1400 Å, to match the SMOV measurement, and 2700 Å, to measure the scattered light at a wavelength not previously observed.

2. Observations

GHRS Cycle 5 calibration program 6210 obtained spectra of the star HD 106343 (B1.5Ia) with the first-order gratings G160M and G270M using RAPID mode. The central wavelength for the G160M observation was 1400 Å, while the central wavelength for the G270M grating observations was 2700 Å. To complete the scan without interruption, the target star was observed in the CVZ. The star was successfully acquired with an LSA ACQ and SSA ACQ/PEAKUP using mirror N2. The G160M observations completed successfully. Due to a carrousel problem, the G270M observations did not execute and were rescheduled before the February 1997 Servicing Mission. A summary of the successfully executed observations is presented in Table 1.

The observing plan for program 6210 was to center up on the star, back off 0.2 arcsec, and scan across the star out to a radial distance of 3.0 arcseconds. The first dwell position at radial distance of –0.2 arcsec from the SSA acquisition position was chosen so the scan would sample both sides of the PSF. A scan with nine dwell positions was defined. The target was centered in the SSA with an ACQ/PEAKUP before the start of each SCAN. Three SCANs were obtained, two were in the $-x$ direction at a wavelengths of 1400 Å and 2700 Å and one was in the $+y$ direction at 2700 Å.

Table 1: Observation Summary

Visit	Observation	Wavelength (Å) & grating	Scan Direction	Obs. Date
1	z33c0106	1400 (G160M)	$-x$	21-DEC-1996
2	z33c0208t	2700 (G270M)	$-x$	5-FEB-1997
2	z33c020et	2700 (G270M)	$+y$	5-FEB-1997

3. Inspection of the Spatial Scans

There are a minute or so of RAPID readouts at the first dwell position before the start of each spatial SCAN. This is normal and was expected. Also, the last dwell position for each spatial SCAN has fewer than the requested number of RAPID readouts. This anomaly is a known bug.

Inspection of SCAN #1 (z33c0106t) in the –*x*-axis direction indicated RAPID readouts occurred at the desired dwell positions as well as during the movement of the aperture between each dwell position. There was a gap in the engineering telemetry during dwell #2. A peak in the data occurred during dwell #2 that could be due to spacecraft jitter. The corresponding RAPID readouts were not used in the sum. In addition, there is about 1 minute of RAPID readout data during dwell #4 that are mostly noise compared to the counts in the other readouts. There is no evidence to support a recentering event (movement of the star out of the aperture) during dwell #4 to explain the low counts. The low counts could result from an unknown anomalous instrument problem. This is unlikely because the hot diode on Side 2 is present in the raw data. This anomaly is under investigation.

Inspection of SCAN #2 (z33c0208t) in the –*x*-axis direction indicated RAPID readouts occurred at the desired dwell positions as well as during the movement of the aperture between each dwell position. A peak in the OMS data occurred during dwell #7 that could be due to spacecraft jitter.

Inspection of SCAN #3 (z33c020et) in the +*y*-axis direction indicated RAPID readouts occurred at the desired dwell positions as well as during the movement of the aperture between each dwell position. However, there was a gap in the engineering telemetry before the end of the previous SSA ACQ/PEKUP (z33c020at) which did not end until after the spatial scan. Therefore, there is no OMS information about the RA and DEC of the aperture during this time period.

4. Data Reduction

The OPUS pipeline calibration is not appropriate for this program, and the observations were recalibrated off-line using the STSDAS task **calhrs**. A minimum number of calibration switches were set to PERFORM to obtain the number of detected counts at each dwell position. All other calibration switches were set to OMIT. The selected calibration switches are presented in Table 2. Even though calibration switches PPC_CORR, PLY_CORR, and BCK_CORR were set to PERFORM, these calibration steps were not performed. No paired pulse correction (PPC_CORR) was performed because the data was not converted to count rate, EXP_CORR=OMIT (division by exposure time). The background correction (BCK_CORR and PLY_CORR) was not performed because dispersion constants were not applied.

The STSDAS task **gstatistics** was used to sum the detected counts in the corresponding groups for each dwell position. For example, the SCAN #1 observation (z33c0106t) contains 4432 raw data groups while the calibrated data has 4429 groups of data. A total of 474 groups (out of the expected 480 groups) at each dwell position were summed, except for dwell position #9. A few RAPID readouts were excluded from the sum at dwell position #2 due to a spurious data spike which possibly resulted from high jitter during an

engineering gap. Dwell position #9 had fewer than the expected number of groups. This anomaly of fewer than expected number of RAPID readouts results from a known bug. The groups used in the sum and the total counts summed at each dwell position is presented in Table 3. For each dwell position, the starting and ending groups are presented in the table. The starting and ending groups could only be determined for the first few groups with high counts, while the groups used in the sum for following dwell positions were extrapolated. A comparison of the summed counts at each dwell position relative to the dwell position with the most summed counts is presented in column “Relative Counts”.

Table 2: z33c0106t - Calibration Switches

Switch	Value	Comment
DQI_CORR	PERFORM	data quality initialization
EXP_CORR	OMIT	division by exposure time
DIO_CORR	PERFORM	diode response correction
PPC_CORR	PERFORM	paired pulse correction
MAP_CORR	PERFORM	mapping function
DOP_CORR	OMIT	doppler compensation
PHC_CORR	PERFORM	removal of photocathode nonuniformity
VIG_CORR	PERFORM	removal of vignetting nonuniformity
MER_CORR	PERFORM	merging of substep bins
GWC_CORR	OMIT	use global wavelength coefficients
ADC_CORR	OMIT	application of dispersion constants
MDF_CORR	OMIT	median filter of background spectra
MNF_CORR	OMIT	mean filter of background spectra
PLY_CORR	PERFORM	polynomial smoothing of background spectra
BCK_CORR	PERFORM	background removal
IAC_CORR	OMIT	incidence angle correction
ECH_CORR	OMIT	correction for echelle ripple
FLX_CORR	OMIT	absolute flux calibration
HEL_CORR	OMIT	conversion to heliocentric wavelength
VAC_CORR	OMIT	vacuum to air correction

Observation z33c0208t (G270M) was obtained with a scan of 70 groups/dwell position, while observation z33c020et (G270M) was obtained with 160 groups/dwell position.

Two non-CVZ orbits were used to repeat the G270M observations. Observation z33c0208t was in the first orbit with the target acquisition and has fewer groups/dwell position than observation z33c020et. The groups used in the sum and the total counts at each dwell position are presented in Tables 4 and 5.

Table 3: z33c0106t - HD 106343

Dwell Position	Groups Summed	Total Counts	Relative Counts	Position (*x*-axis)
1	80-466, 473-560	130417.0	0.590	+0.2
2	578-880, 886-1058	220286.0	1.000	–0.2
3	1066-1225, 1231-1546	22370.3	0.101	–0.6
4	1554-1690, 1696-2034	2585.82	0.0117	–1.0
5	2042-2305, 2311-2522	2853.74	0.0129	–1.4
6	2530-3000, 3006-3010	3764.55	0.0170	–1.8
7	3018-3215, 3221-3498	3185.69	0.0144	–2.2
8	3506-3716, 3722-3986	2379.52	0.0108	–2.6
9	3994-4429	2214.94	0.0100	–3.0

Table 4: z33c0208t - HD 106343

Dwell Position	Groups Summed	Total Counts	Relative Counts	Position (*x*-axis)
1	61-69, 75-135	116734.0	1.000	+0.2
2	170-238	112429.0	0.963	–0.2
3	248-316	7037.64	0.060	–0.6
4	326-394	3269.17	0.0287	–1.0
5	404-472	826.598	0.0071	–1.4
6	482-550	648.43	0.0056	–1.8
7	560-628	444.995	0.0037	–2.2
8	638-706	446.686	0.0038	–2.6
9	716-741	174.972	0.0015	–3.0

Table 5: z33c020et - HD 106343

Dwell Position	Groups Summed	Total Counts	Relative Counts	Position (*y*-axis)
1	83-89, 94-250	138853.0	0.1447	–0.2
2	258-420	959264.0	1.000	+0.2
3	428-590	14928.0	0.0155	+0.6
4	598-760	12118.9	0.0126	+1.0
5	768-930	3523.63	0.0036	+1.4
6	938-1100	1682.64	0.0017	+1.8
7	1108-1270	1209.67	0.0013	+2.2
8	1278-1440	1133.06	0.0012	+2.6
9	1448-1550	614.862	0.0006	+3.0

Figure 1 presents the nine data points for observation z33c0106t (G160M), log (counts) versus dwell position. The plot represents the outline of the GHRS PSF envelope, sampled with the SSA (0.22 arcsec square) at a spacing of 0.4 arcsec. The counts for dwell position #9 have been scaled to match the number of summed groups for the other dwell positions.

5. HST Pointing and Slew Positions

The scans did not start at the peak of the PSF. Following the SSA ACQ/PEAKUP, the aperture was offset 0.2” from the initial position. The positioning of the target star relative to the SSA (centering error and the positioning error of the aperture) during the scan (dwell steps) will be the limiting factor in determining the location of the star relative to the spatial scan, and ultimately the usefulness of the 6210 observations.

The error in the spacing of the dwell positions is a function of the Faint Guidance Sensors (FGS) geometric distortion. The FGS operational optical field distortion error is ~10 milliarcsec per arcmin, or ~1 milliarcsec over a few arcsec. This indicates the spacing between the dwell positions is very good.

The Observatory Management System (OMS) data table (`.cmi` or `.jit`) contains information about the spacecraft pointing during an observation (i.e., V2 and V3 axis, V2 and V3 RMS error, RA and DEC, Latitude and Longitude...). The positions of the aperture (RA and DEC) contained within the `.jit` table are calculated from the positions of the FGS star selector servo relative to the GHRS aperture and the positions of the selected guide stars from the Guide Star Catalogue (GSC). The relative positional error for a single

star from the GSC range from 0.3 to 0.8 arcsec, depending upon hemisphere and magnitude (Taff et al. 1990). The target star HD106343 is a bright star (m_V ~6.22) in the southern hemisphere and Hipparcos Input Catalogue coordinates were used for acquisition. The target coordinates are not in the HST Guide Star reference frame and the LSA ACQ followed by an SSA ACQ/PEAKUP should have minimized any positional errors. GHRS-ISR-079, “Interpreting GHRS Target Positioning”, presents with examples a description of GHRS target acquisitions and how to check the pointing of *HST* during an observation. A description of OMS products can be found in the *HST Data Handbook*.

Inspection of the Visit 01 SSA ACQ/PEAKUP (from the OMS Observation Logs) shows a shaky appearance to the spiral search pattern. A possible “false fine lock” may have occurred during the SSA ACQ/PEAKUP. Discussions with an FGS scientist indicates no “false fine lock” occurred. The shaky appearance of the spiral search is due to the OMS sample rate. Also, a check of the FGS walk down on the guide star pair during FGS guide star acquisition clearly shows the stars are single point sources. The spacing between dwell positions should have been 0.4 arcsec. This was confirmed. Dwell position 6 shows an anomalous RA and DEC in the OMS table, which is under investigation.

The RA and DEC positions of the aperture for the G160M and G270M –*x*-axis scans from the OMS tables are presented in Tables 6 and 7. There is no OMS table for SCAN 03 (+*y*-axis scan) during Visit 02 due to a gap in the engineering telemetry.

Table 6: Visit 01 X-axis Scan Positions

rootname	OMS-RA	OMS-DEC	ΔRA[a] (arcsec)	ΔDec (arcsec)	Δ (arcsec)
z33c0104j	183.5709204	-64.40841131	—	—	—
z33c0106j	—	—	—	—	—
1	183.5709978	-64.40845514	–0.120	0.157	+0.198
2	183.5708423	-64.40836702	0.121	–0.159	–0.200
3	83.5706823	-64.40827924	0.370	–0.475	–0.602
4	183.5705252	-64.40819085	0.614	–0.793	–1.00
5	183.5703671	-64.40810359	0.860	–1.107	–1.402
6	183.5702094	-64.40801578	1.105	–1.423	–2.027
7	183.5700513	-64.40792813	1.351	–1.739	–2.202
8	183.5698945	-64.40783974	1.595	–2.057	–2.603
9	183.5697339	-64.40775173	1.845	–2.374	–3.007

a. Multiplied by cos δ.

Table 7: Visit 02 X-axis Scan Positions

rootname	OMS-RA	OMS-DEC	ΔRA[a] (arcsec)	ΔDEC (arcsec)	Δ (arcsec)
z33c0204j	183.5713555279886	-64.408390681568421	—	—	—
z33c0208j	—	—	—	—	—
1	183.5713846171119	-64.40844519946145	–0.045	0.196	+0.201
2	183.5713290350754	-64.40833711251114	0.041	–0.192	–0.197
3	183.5712734794718	-64.40822877026082	0.127	–0.582	–0.596
4	183.5712166158389	-64.40811955755859	0.216	–0.976	–0.999
5	183.5711611394288	-64.40801170327659	0.302	–1.364	–1.397
6	183.5711279783978	-64.40794529859187	0.354	–1.603	–1.641
7	183.5710506412065	-64.40779440372674	0.474	–2.146	–2.198
8	183.5709934630883	-64.40768561500021	0.563	–2.538	–2.599
9	183.5709385473635	-64.40757727396206	0.648	–2.928	–2.999

a. Multiplied by cos δ.

The OMS-RA and -DEC positions of the aperture during the spatial scans (except for position 6) verify that the SCAN executed as commanded and the requested stepping was obtained during the scan. The time stepping in seconds from the start of the OMS window contained within the OMS table is too large to be able to correlate this time with the packet times of the individual data groups in the SCANs. The OMS products are not sufficient for this purpose.

A comparison between Visit 01 and 02 OMS-RA and -DEC of the aperture at the end of the SSA ACQ/PEKAUPs shows ~0.6 arcsec difference in the position of the aperture. This result is larger than expected. A check of the Yale Double Star Catalogue indicates the target star is not a double star. During Visit 01, FGS 01 & 02 were used for acquisition, while FGS 01 & 03 were used for the second visit. A check of the FGS walk downs for both pairs of guide stars indicates all four guide stars are single. The 0.6 arcsec difference in position can only be explained as the accumulation of GSC positional errors. Therefore, the OMS-RA and -DEC at the end of the SSA ACQ/PEAKUPs can not be used to determine the position of the star relative to the scans. Information about the SSA acquisition and guide stars are presented in Tables 8 and 9.

Table 8: Target Positions during Visits 01 and 02

SSA ACQ/ PEAKUP	OMS-RA	OMS-DEC	Mirror	MAPFND	FLUXFND
z33c0104t	183.5709204	-64.40841131	N2	9	52885.0
z33c0108t	—	—	N2	8	53162.0
z33c010ct	183.5709364	-64.40840336	N2	2	52809.0
z33c0204j	183.5713555279886	-64.408390681568421	N2	8	52598.0
z33c020at	—	—	N2	14	50771.0

Table 9: Guide Star Positions for Visits 01 and 02

SSA ACQ/ PEAKUP	GSD_RA	GSD_DEC	GSD_MAG	PREDGSEP (arcsec)	ACTGSSEP (arcsec)
z33c0104j	—	—	—	—	—
0898201326	183.45744	-64.23999	10.316	—	—
0898202730	183.74770	-64.54285	9.481	1180.131	1180.274
z33c0208j	—	—	—	—	—
0898200642	184.21008	-64.24233	11.007	—	—
0898202408	183.59258	-64.55769	11.067	1487.069	1486.713

6. Fitting GHRS Spatial Scan with Model PSF Pattern

There should be symmetry about the SSA ACQ/PEAKUP position of the star and the spatial scan. However, due to SSA centering errors, the position of the star is not known to the desired accuracy. The answer to the star positional question can be found by determining graphically the position of the star. The solution is to fit a model PSF pattern to the GHRS spatial scan points. The differences between the model fit and the actual data points will be a direct measure of the centering errors. We should inject a note of caution at this point: one of the frailties of this approach is the assumption that the GHRS PSF is symmetric. This approach does not take proper regard of PSF variations.

The light entering the FOC (OTA+COSTAR) will be a close match to the light entering the GHRS. Model FOC PSF images were created using TinyTim. Models were created to match the GHRS 1400 Å (FOC F140M filter) and the 2700 Å (FOC F278M filter) observations. The FOC model PSF pixel scale is 0.0143 arcsec (f/96). A square aperture (15 pixels on a side) was walked across the model PSF images to match the scan positions of the GHRS observations. A plot of the sum of the counts in this aperture at each position

should represent the measured PSF envelope extracted from the GHRS observations. The model points were scaled to match the GHRS second dwell position points.

A good match was found between the FOC model scan points and the first four GHRS dwell positions in each scan. Beyond dwell position #4 (1.0 arcsec), the counts in the model scan continue to fall off in intensity while the counts in the GHRS scan level off. The GHRS profile beyond 1.0 arcsec suggests higher scattered light than is predicted by the FOC PSF model. It is unlikely that these profile wings are due to detector noise because the counts detected are significant and well above normal background levels.

For each FOC model image, the first scan of the square aperture duplicated the commanded GHRS scan positions. For each successive scan, the aperture was offset either to locate dwell position #2 closer or farther from the peak of the model PSF. For the GHRS 1400 Å –*x*-axis spatial scan, a good match was found between the model and the actual data points if the model dwell position #2 was moved one FOC pixel closer to the PSF peak pixel. This movement translates into an error of ~0.014 arcsec for the GHRS aperture. It was found that a 1 pixel shift, pushing dwell position #2 away from the PSF peak pixel, resulted in a good match to the GHRS 2700 Å –*x*-axis scan (~0.014 arcsec error). For the GHRS 2700 Å +*y*-axis scan, a 3 pixel shift closer to the FOC PSF peak was close to matching the GHRS scan, but on the high side of the curve. A shift of 4 FOC pixels was too much of a shift resulting in falling below the +*y*-axis scan. Therefore, the best shift would have been ~3.5 pixels. A summary of the relative centering errors is presented in Table 10.

Table 10: Fitting GHRS Spatial Scan with Model FOC PSF Pattern

Dwell Scan	GHRS Wavelength	FOC filter	Relative pixel Shift	Offset Error (arcsec)
–*x*-axis	1400 Å	F140M	1	~0.014
–*x*-axis	2700 Å	F278M	1	~0.014
+*y*-axis	2700 Å	F278M	~3.5	~0.050

Figure 2 presents the scaled model FOC scan points (dashed line) overlaid upon the respective GHRS scan points (solid line) for the –*x*-axis scan. Figure 3 presents the scaled model fit for shifts of 3 and 4 pixels for the +*y*-axis scan. The positions of the points have not been corrected for the relative error. The plots show a relatively good fit for the first four dwell positions between the FOC model and the actual GHRS data points. And, it shows the fall off in intensity of the FOC model PSF relative to the GHRS measurements at greater distances.

7. Conclusions and Recommendations

The FOC model fit, of course, is not intended to represent the actual GHRS PSF, but instead to determine the position of the star relative to the GHRS scan. However, comparisons of the FOC model scans with the actual GHRS scans do show some similarities as well as some discrepancies that are worth noting.

First, the –*x*-axis scans indicate the GHRS PSF within the region <1.0 arcsec is slightly broader at 1400 Å than at 2700 Å. This broadening of the profile may be due to a halo effect at 1400 Å that is not present at 2700 Å. This broadening appears to be in both the actual GHRS scans and the FOC model scans which suggests it is possibly related to the COSTAR optics. The 1400 Å scan starts to diverge from the FOC model at ~1.0 arcsec, while the 2700 Å scan tracks the FOC model scan out to a distance of ~1.4 arcsec before diverging from the model scan. This would indicate the onset of scattering is more pronounced at 1400 Å than at 2700 Å.

Second, the +*y*-axis scan at 2700 Å shows a narrower inner core to the profile compared to the –*x*-axis scan profiles. This result is possibly due to the inferred large offset (~0.050 arcsec) introduced in the positioning of the +*y*-axis spatial scan. This only indicates the target star was more centered in the aperture at dwell position #2 for the +*y*-axis scan than for the –*x*-axis scans. If the +*y*-axis and –*x*-axis scans at 2700 Å are overlaid and moved vertically so as to match the counts at dwell position #4, the fall off in the profiles are nearly identical. This suggests the far wings of the PSF are symmetrical at 2700 Å. The –*x*-axis scan, which has better positioning to measure the wings of the PSF, is a good indicator of the fall off in the wings of the GHRS PSF.

The observations at both 1400 and 2700 Å demonstrate that the GHRS PSF has extended wings. These do not rise above the “expected” (FOC) level until one is at about 1% of the peak intensity for a star, therefore these wings are unlikely to contaminate the spectrum of a nearby star in a significant way except when there is a large (~5 magnitude) difference in brightness. The information provided in the figures and tables should allow a first-order correction to be made in such cases if spectra of both objects exist.

8. References

Taff L., et al. 1990, Ap.J., 353, L45.

Figure 1: Observed number of counts for each dwell point for observation z33c0106t with grating G160M.

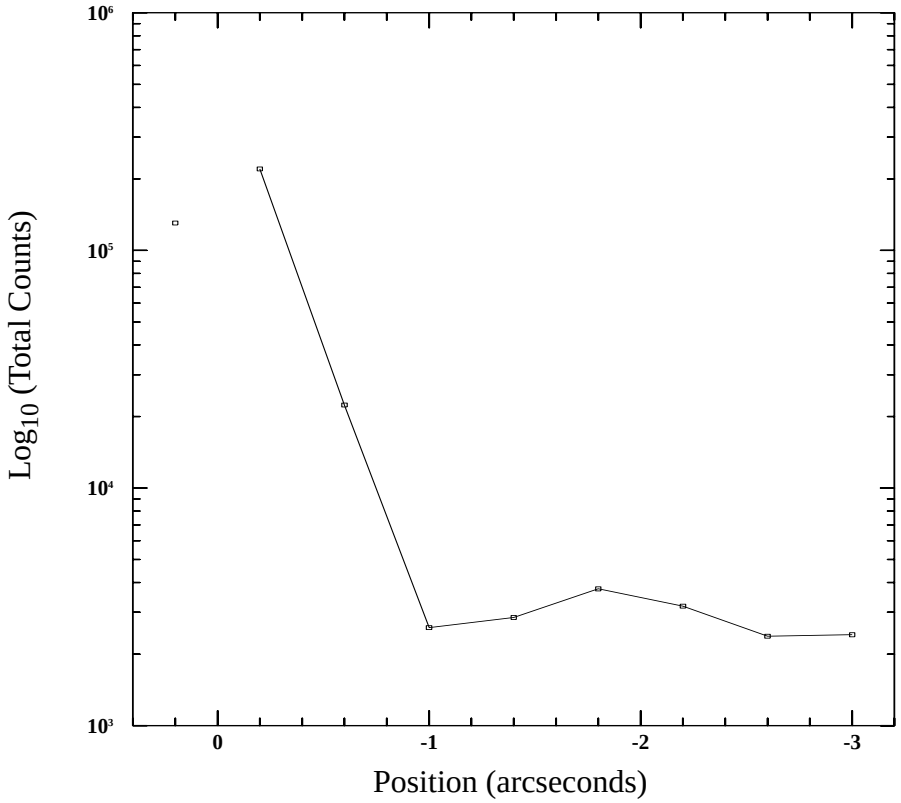

Figure 2: Comparison of observed GHRS profiles with models from TinyTim that used FOC parameters. Upper: G160M profile (solid line) compared to FOC F140M filter (dashed line), offset by one pixel. Lower: G270M profile (solid line) compared to FOC F278M filter (dashed line), offset by one pixel.

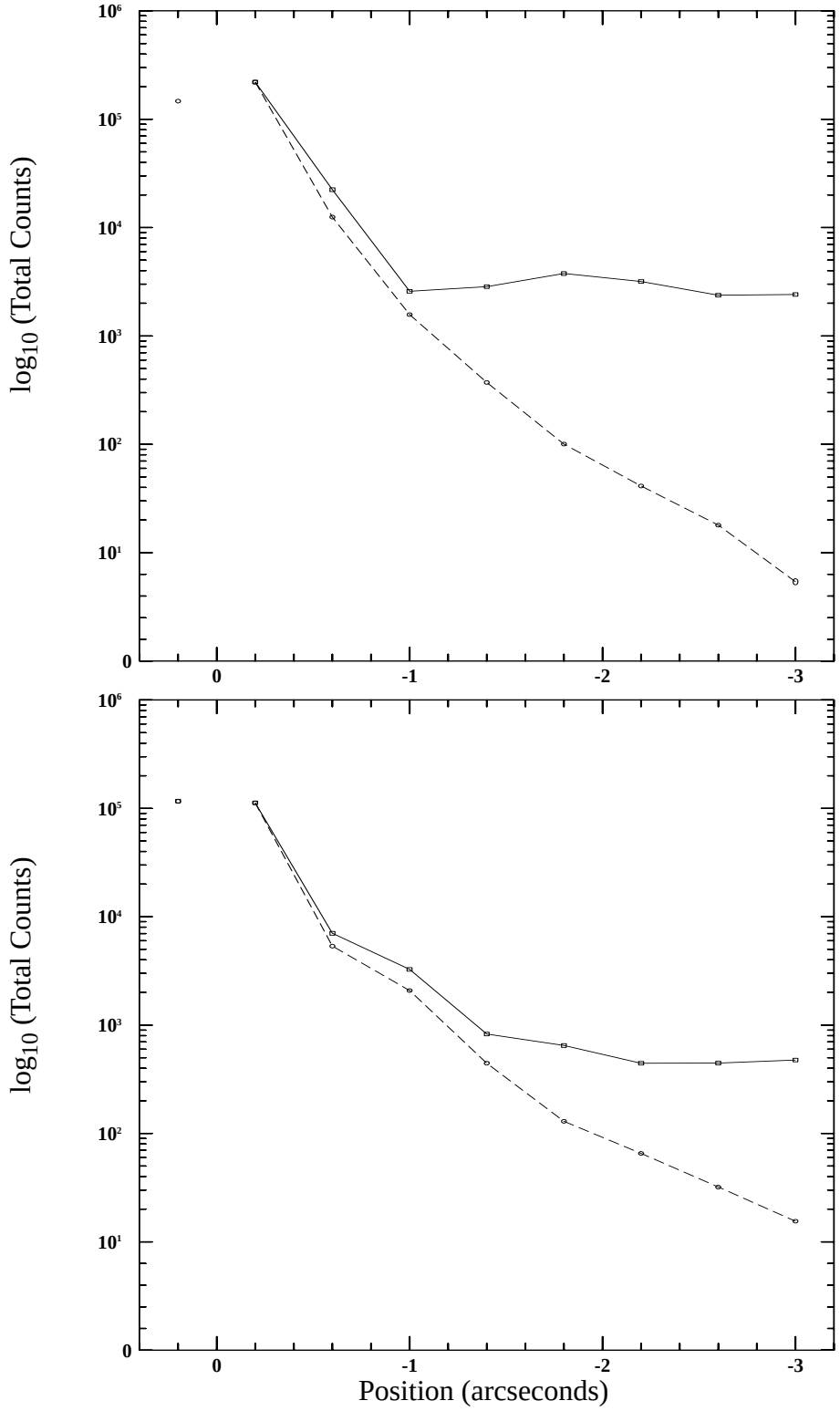

Figure 3: A comparison of GHRS G270M *y*-axis scans to models for the F278M filter of the FOC. The upper has the FOC profile offset by 3 pixels, while for the lower the offset is 4 pixels.